ACS NANO

www.acsnano.org

ARTICLE

Size-Selective Sub-micromter-Particle Confinement Utilizing Ionic Entropy-Directed Trapping in Inscribed Nanovoid Patterns

Long Chen, Ashwin Panday, Jonggab Park, Mingyu Kim, Dong Kyo Oh, Jong G. Ok,* and L. Jay Guo*

Cite This: https://doi.org/10.1021/acsnano.1c00014

Read Online

ACCESS | Metrics & More | Article Recommendations | Supporting Information

ABSTRACT: **We have developed a single-step, high-throughput methodology to selectively confine sub-micrometer particles of a specific size into sequentially inscribed nanovoid patterns by utilizing electrostatic and entropic particle−void interactions in an ionic solution. The nanovoid patterns can be rendered positively charged by coating with an aluminum oxide layer, which can then localize negatively charged particles of a specific size into ordered arrays defined by the nanovoid topography. On the basis of the Poisson−Boltzmann model, the size-selective localization of particles in the voids is directed by the interplay between particle−nanovoid geometry, electrostatic interactions, and ionic entropy change induced by charge regulation in the electrical double layer overlapping region. The underlying principle and developed method could potentially be extended to size-selective trapping, separation, and patterning of many other objects including biological structures.**

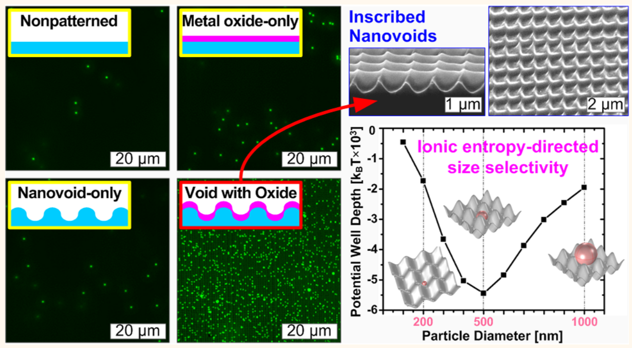

KEYWORDS: *continuous nanoinscribing, nanovoid, size-selective particle confinement, electrostatic interaction, ionic entropy, electrical double layer*

Particles of micro- and nanoscale sizes have drawn significant research interests due to their versatile functionalities such as interactions with light[1−3] and molecules,[4,5] high catalytic activity,[6−8] and quantum confinement effect.[9,10] In particular, if particles of a certain size can be placed in the array format, many practical applications can be exploited including photonic crystals,[11−13] nanoelectronic devices,[14−16] optical switches[17,18] and filters,[19,20] filtration devices,[21] and biological assays.[22−24] However, it is often tedious and energy-consuming to create controlled particle patterns using conventional subtractive micro- and nanofabrication processes.[25,26] Size-selective particle confinement, separation, and sorting are highly desired in various applications such as diagnostics, chemical and biological analyses, food and chemical processing, and environmental assessment.[27] Those have been implemented by many methods including pinched flow fractionation,[28] lateral displacement sorting,[29] hydrodynamic chromatography,[30] (di)electrophoresis (DEP),[31,32] and other magnetic, optical, and acoustic manipulation techniques.[27] While effective, most of these methods require continuous driving flow and complicated streamline and channel design, and usually work for particles with sizes in tens to hundreds of micrometers. Hence, separation and sorting sub-micrometer-sized particles and biological objects with high throughput are still very challenging. Another widely exploited strategy is to utilize the more scalable self-assembly of particles.[33−35] While the self-assembly processes relying on "particle−particle interaction" have nicely worked for setups such as particle-trapping floating electrodes in microfluidic DEP cells[36] and their interaction force measurement systems,[37] assembly into high-density arrays and with desired patterns is still tough.

To address the above issues, in this work we present a low-cost yet highly scalable methodology of trapping of particles of selective sizes at desired positions. Specifically, we create a "nanovoid" pattern on a substrate and exploit a topography-specific interaction between particles and nanovoids, which localizes the particles of the right sizes to the prepatterned

Received: January 1, 2021
Accepted: August 2, 2021

lattice sites. Fabrication of the microscale well arrays as particle-trapping templates through conventional nanofabrication approach has been demanding and often of poor reproducibility due to complex mask design, tricky etching, and limited area.[38] However, a high-throughput and scalable fabrication of the nanovoid patterns could be implemented by using two-dimensional dynamic nanoinscribing (2D-DNI) comprised of sequential continuous mechanical inscribing strokes.[38−41] By exploiting geometry-induced electrostatic interaction[42−45] between charged particles and the nanovoid array in ionic solution, we achieved topography-directed, position-selective localization of particles, arranging particles at positions that are predefined by the nanovoid topography and surface charge, instead of randomly depositing them on the substrate. We further elucidate that the "well" depth of the total free energy is contributed by the ionic entropy as well as the electrostatic potential between a particle and void surface. The patterning of substrate and size-selective confinement realize orderly localization of particles beyond random filling of the voids.

RESULTS AND DISCUSSION

Microfluidic Nanovoid Device Development. The proposed nanostructured 2D void pattern with sinusoidal profile was created by DNI on a polymer film; as schematically illustrated in Figure 1a. To perform DNI, a well-cleaved rectangular nanograting mold edge (Figure 1b) is brought in contact with the substrate at a proper angle and force, and then slides over the substrate while maintaining a conformal contact. The concentrated stress at the dynamic contact regions on the polymer film causes plastic deformation of the polymer to form nanograting structure with controlled profiles (Figure 1c).[39,41] The DNI strokes can be sequentially repeated in the orthogonal direction to produce the 2D sinusoidal nanovoid pattern (Figure 1d).[38,40] In DNI, the pattern period is dictated by that of the grating mold, and thus nanovoids of specific sizes (*i.e.*, depending on the target particles to selectively catch) can be precisely created by 2D-DNI in a continuous and scalable fashion at high speed (∼1 m/min or faster), which is not available by other conventional techniques. For instance, we used a 700 nm period SiO_2 grating mold for the 700 nm diameter nanovoid patterning on polycarbonate (PC) substrates in this work (unless otherwise noted). The morphologies of the sinusoidal voids created by 2D-DNI can be further tailored by changing the substrate material, applied force, processing temperature, and inscribing speed.[41]

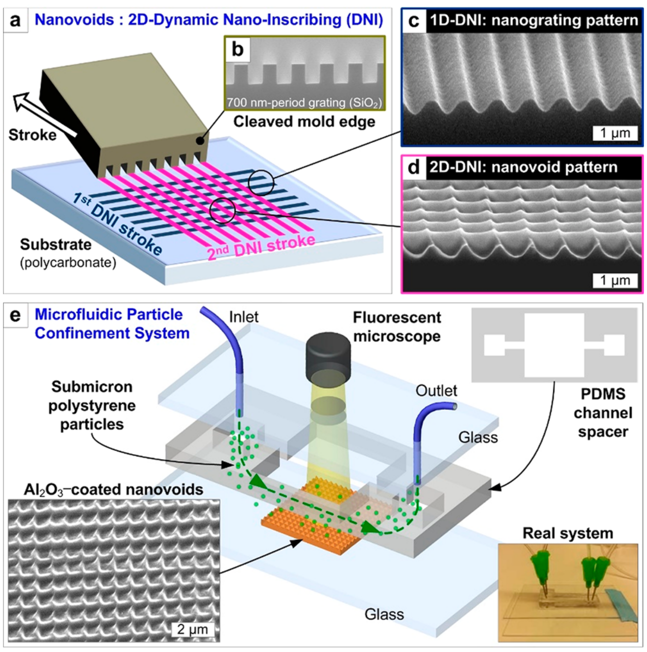

Figure 1. (a) Schematic illustration of the dynamic nanoinscribing (DNI) patterning technique. (b) Well-cleaved rigid mold containing desired nanograting pattern, continuously sliding over the substrate under conformal contact and controlled heating. (c) Single DNI stroke producing the 1D nanograting pattern with a sinusoidal cross-section profile. (d) Two DNI strokes combined along orthogonal directions, creating the 2D nanovoid pattern. (e) Microfluidic device designed for particle confinement. A fluidic cell chamber consists of two transparent slide glasses spaced by the poly(dimethylsiloxane) (PDMS) block having a slit channel. The oxide-coated nanovoid pattern is mounted on the bottom in the fluidic cell chamber, and the fluorescent-labeled particles are injected under the fluorescent microscope.

Figure 1e depicts the experimental setup comprising a microfluidic slit channel chamber and a nanovoid substrate coated with a RF-sputtered 10 nm thick Al_2O_3 layer which is positively charged (surface charge density of +2.06 mC/m^2 from ζ potential measurement) when immersed in an ionic solution (10^{-4} M (mol/L) KCl). As the suspension of negatively charged sub-micrometer polystyrene (PS) particles (surface charge density of −1.6 mC/m^2) flows into the fluidic cell, interestingly, particles are nicely trapped in the voids, depending on their relative sizes. Parametric characterization of surface charge density under varied conditions is presented further in detail in Section S1 in the Supporting Information. The ionic solution, containing the particles fluorescently labeled for ease of visualization, was injected into the chamber and was allowed to equilibrate inside the chamber for 15 min before microscopic observation. Under the fluorescent microscope, we can directly visualize the localization and trapping dynamics of fluorescent-labeled particles in our system. Detailed characterization procedure is described in Methods. The charged particles undergoing Brownian motion in solution experience an electrostatic attraction in the vicinity of the oppositely charged 2D-DNI-patterned surface (*i.e.*, within the Debye screening length; see Size Selectivity for pertinent discussion). As will be demonstrated later, their size and surface charge density control the trapping behavior in the patterned voids.

Surface Charge-Directed Trapping of Sub-micrometer Particles in the Nanovoids. ζ potential measurement shows that the Al_2O_3-coated surface immersed in ionic KCl solution possesses a positive surface charge, which is primarily through the protonation of terminal -OH groups. Figure S1 in Section S1 in the Supporting Information presents this baseline study in detail. Next, we characterize the behavior of negatively charged sub-micrometer PS particles injected in the ionic solution with or without the nanovoid surface. Figure 2a−d shows the microscope images of the 500 nm diameter PS particles (0.1 wt % concentration) trapped on the substrates with different surface conditions in the 10^{-4} M KCl solution. In the absence of the nanovoid pattern on the substrate, only few particles are randomly adsorbed on the surface (Figure 2a), even in the case when surface charges are presented by the Al_2O_3 layer (Figure 2b). The bare nanovoid surface with no

https://doi.org/10.1021/acsnano.1c00014
ACS Nano XXXX, XXX, XXX−XXX

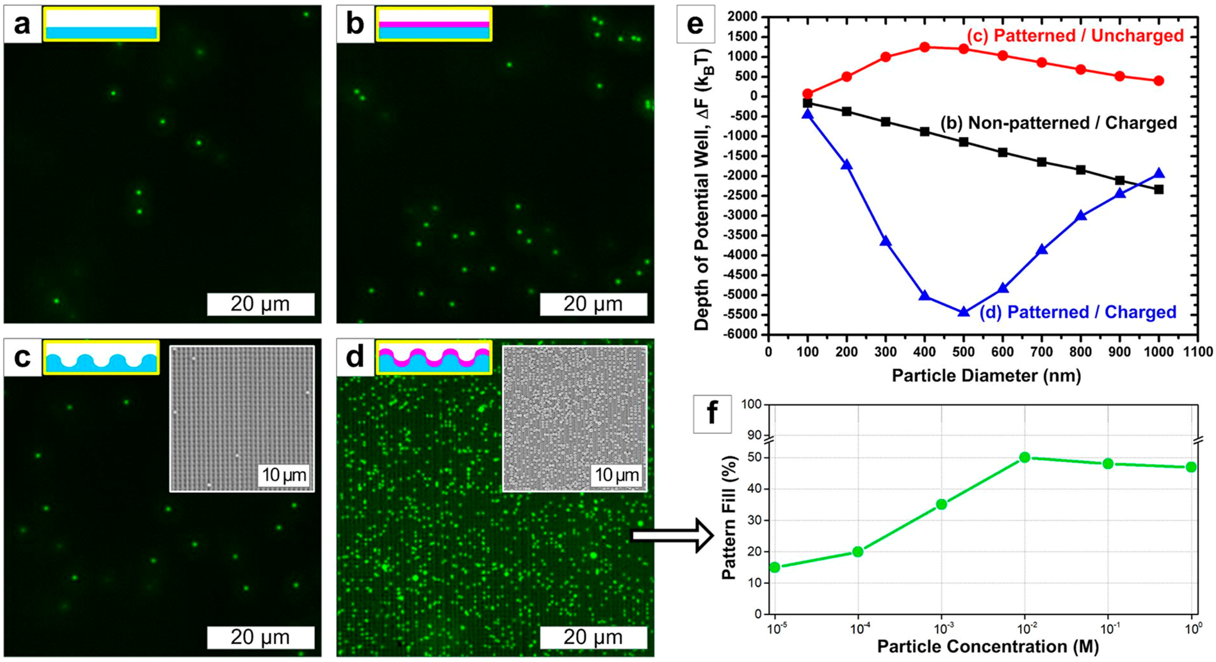

Figure 2. Epi-fluorescent micrograph images of 500 nm diameter particles on a nonpatterned, bare (noncoated) polycarbonate (PC) substrate (a), nonpatterned, 10 nm thick Al_2O_3-coated PC substrate (b), nanovoid-patterned, bare (noncoated) PC substrate (c), and nanovoid-patterned, 10 nm thick Al_2O_3-coated PC substrate (d). Upper-side illustrations depict the schemes of each surface. Insets, panels c and d: scanning electron microscopy (SEM) images of respective cases, clearly comparing the amounts of particles trapped in the nanovoids without or with Al_2O_3 coating. (e) Calculated potential wells as a function of particle diameters for cases b−d. (f) Nanovoid fill ratio as the function of the particle concentration for case d.

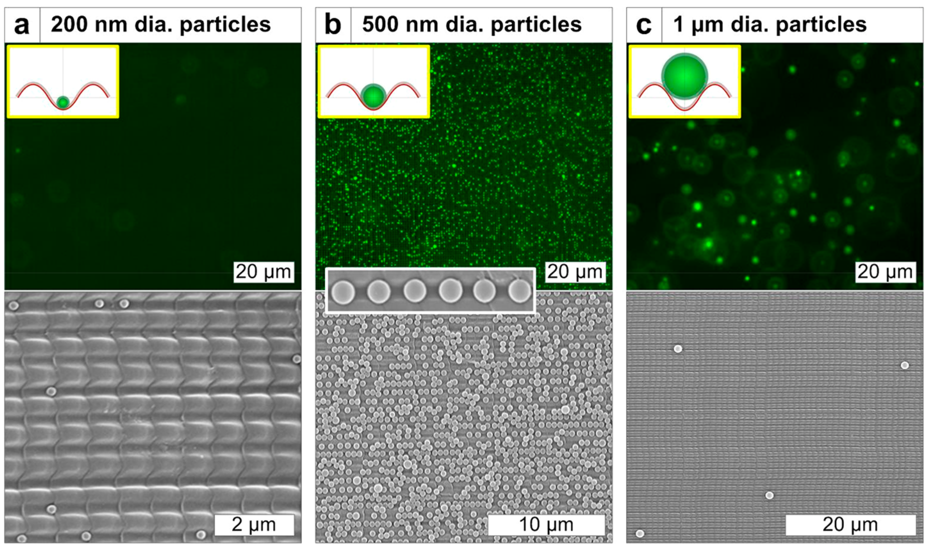

Figure 3. Fluorescent microscope images (top row) and SEM images (bottom rows) of the particles trapped to the Al_2O_3-coated nanovoid structures, with the diameters of 200 nm (a), 500 nm (b), and 1 μm (c). The upper-left insets show the schemes of each case. The middle inset to panel b shows the enlarged SEM image disclosing the 500 nm diameter particles trapped in nanovoids in an orderly fashion.

Al_2O_3 coating also shows ineffective particle confinement (Figure 2c). Finally, when the nanovoid surface is coated with the Al_2O_3 layer, a much larger number of particles are trapped onto the substrate (Figure 2d). Almost all trapped particles are well-confined inside the nanovoids. The confined particles strongly adhere to the surface and cannot be removed by rinsing the channel with DI water. Only by using stronger physical force such as sonication can particles be dislodged from the surface.

This nanovoid topography-directed nanoparticle confinement will be further discussed in the following sections *via* the theoretical modeling and simulation of total free energy including both electrostatic and entropic contributions of the nanoparticle−nanovoid system. Briefly, the depth of the free energy well was calculated for the three cases as shown in Figure 2e: nonpatterned-charged (Figure 2b case), patterned-uncharged (Figure 2c case), and patterned-charged (Figure 2d case). As will be detailed in the next section, the potential wells were calculated as the free energy change of the system (see eq

https://doi.org/10.1021/acsnano.1c00014
ACS Nano XXXX, XXX, XXX−XXX

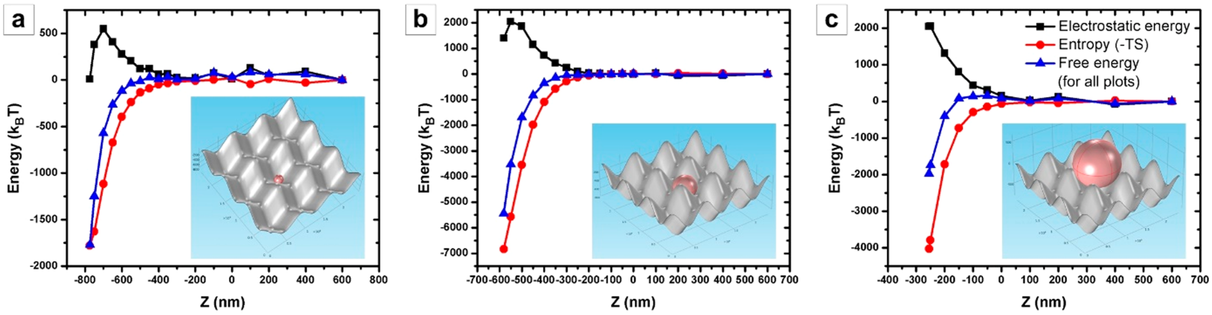

Figure 4. Energy change of the system, calculated by simulating that particles are approaching to the bottom of the void in the *z*-direction (normal to the void depth), for the particles with the diameters of 200 nm (a), 500 nm (b), and 1 μm (c). Insets to each plot show the particles at the lowest positions in the voids, modeled for simulation.

6) as the particle approaching the substrate surface from a far distance, as demonstrated in Figures 4 and 5. Figures S4, S5, and S6 are also based on the same conditions. This analysis confirms that only the patterned-charged case provides the effective potential well for the 500 nm diameter nanoparticle trapping, suggesting that the size-selective particle confinement is attributed to the combined effects of surface charge and surface geometry.

In order to improve the trapping efficiency and particle pattern quality, we study how the particle concentration affects the void pattern fill ratio. As this process is diffusion-limited and no external stimulus is applied, increasing the particle concentration increases the fill ratio to a certain degree. Further increasing the particle concentration beyond 1 wt % seems not to appreciably increase the fill ratio, as shown in Figure 2f. The fill ratio is saturated at around 50%, which can be possibly explained due to the electrostatic repulsion from the particles already confined on the surface. This suggests that the fill ratio can be enhanced by increasing the interspacing between individual nanovoids or by increasing the attractive particle−substrate interaction by increasing the nanovoid surface charge density.

Size Selectivity: Experimental and Analytic Studies. While we have confirmed above that the 500 nm diameter particles are effectively trapped in similarly sized voids , we have also carried out a series of control experiment with a fixed void size (*i.e.*, ∼700 nm pitch), but three different particle sizes (diameters of 200 nm, 500 nm, and 1 μm) to evaluate the size-dependent trapping behavior. Under similar conditions and at the same mentioned flow rate, we found that only particles of 500 nm diameter were densely confined in the voids (Figure 3b). In the case of 200 nm diameter particles, only some nonspecific adsorption was observed in the patterned voids (Figure 3a). A similar result was observed when testing 1 μm diameter particles (Figure 3c). These results indicate the size-selective nature of this method and provide the possibility for sub-micrometer-sized particle separation and sorting on the basis of their size and surface charge.

To understand this size-selective behavior, we modeled the nanoparticle−nanovoid system and simulated the interaction between the charged particles and the charged void surface using finite element analysis (FEA) method in COMSOL Multiphysics. We calculated the free energies for this system on the basis of the mean field Poisson−Boltzmann (PB) theory[46] and analyzed in detail the electrostatic and entropic contributions as a function of the particle position above the patterned structure.

The electrostatic potential contributed by both surface charges and ions can be calculated by the dimensionless PB equation,

$$\nabla^2\psi = \kappa^2 \sinh(\psi) \tag{1}$$

where $\psi = \frac{e\varphi}{k_B T}$ is the dimensionless electrostatic potential with φ denoting the electrostatic potential, and $\kappa = \sqrt{\frac{2c_0 e^2}{\varepsilon\varepsilon_0 k_B T}}$ with ε denoting the relative dielectric constant of the solvent. κ^{-1} defines the Debye length of the electrical double layers (EDLs) (see Section S2 in the Supporting Information for full derivation).

We assume a fixed surface charge at both surfaces of particle and void structure. The boundary conditions for the potential are defined by the surface charge densities, given by

$$\mathbf{n}\cdot\nabla\psi = -\frac{\sigma}{\varepsilon\varepsilon_0 k_B T} \tag{2}$$

We used surface charge densities of +2.03 and −1.6 mC/m^2 for the substrate surface and particles, respectively, as the same condition in our experiment. These equations were numerically solved using COMSOL Multiphysics. Next we calculated the free energy of the system by taking into account both the energetic and entropic contributions as a function of particle position above the patterned structure. In this simulation the particle's vertical position is referenced from "zero" defined as the position where the particle's bottom point just reaches the void's hilltop point (see insets to Figure 4). The free energy of a charge distribution may be analyzed in terms of its electrostatic potential energy and the configurational entropy of the ions and solvent in the electrolyte. The electrostatic energy of the system is given by[46]

$$U_{es} = \frac{\varepsilon\varepsilon_0}{2}\int_V (\mathbf{E}\cdot\mathbf{E})\,\mathrm{d}V = \frac{1}{2}\int_A \sigma\varphi_s\,\mathrm{d}A + \frac{1}{2}\int_V \rho\varphi\,\mathrm{d}V \tag{3}$$

where φ_s is the potential at the surface and $\rho = \rho^+ + \rho^- = c_0 e[\exp(-\psi) - \exp(\psi)]$ represents the local net charge.

The entropy change of the system is given by (see Section S2 in the Supporting Information for full derivation)

$$\Delta S = k_B \int_V \left\{ \sum_i c_0[z_i\psi\,\exp(-z_i\psi) + \exp(-z_i\psi) - 1] \right\} \mathrm{d}V \tag{4}$$

The integration volumes in both equations are the whole simulation system comprising the charged particles, ions, and

https://doi.org/10.1021/acsnano.1c00014
ACS Nano XXXX, XXX, XXX−XXX

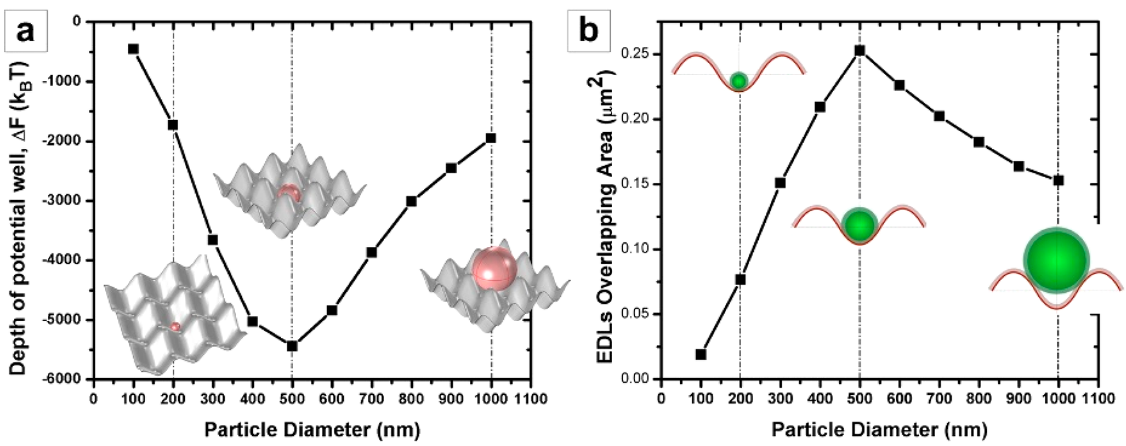

Figure 5. (a) Depth of the free energy potential well for particles in the voids with different sizes. The insets show the geometry of the nanovoids and particles at the lowest positions in the voids. (b) Electrical double layer (EDL) overlapping areas for particles in the voids with different sizes. The insets show the schematics of EDLs overlapping when particles are located at the lowest positions in the voids. Particles with rightsize fitting the void geometry well can obtain the largest EDL-overlapping area, which is 500 nm in this study case.

surface of nanovoids. The system's free energy is then obtained:

$$F = U_{es} - T\Delta S \tag{5}$$

So for our system, we can write the free energy as

$$F = \int_V \left\{ \frac{\varepsilon\varepsilon_0}{2}(\mathbf{E}\cdot\mathbf{E}) - 2c_0k_BT(-\psi\sinh(\psi) + \cosh(\psi) - 1) \right\} \mathrm{d}V \tag{6}$$

Figure 4 shows the calculated energy change of the system, when particles with different sizes approach the bottom of the void in the *z*-direction. Purely from an electrostatic energy standpoint, it could seem counterintuitive that there exists an electrostatic energy barrier preventing the particles reaching the bottom of the voids having opposite charges. The appearance of this electrostatic energy barrier can be more easily understood by considering two parallel charged surfaces. We have provided its detailed derivation and explanation in Section S3 in the Supporting Information for this simpler case: the energy between two charged planar surfaces in an ionic solution derived with the linear PB equation. That is, we could show that even with the linear PB equation, the electrostatic energy barrier was still observed for two oppositely charged planar surfaces at certain spacing, because at this range the increase in the *E*-field and hence the electrostatic energy density is greater than the reduction of the volume between the two surfaces.

Nonetheless, the free energy of the system that governs the final net force and potential experienced by the particles shows a clear attractive interaction between the particle and the voids. The attractive interaction governed by the free energy of the system makes the void behave like a trap, and clearly for the 500 nm diameter particles, this trap has the deepest potential well and strongest confinement as compared to that for the 200 nm and 1 μm diameter particles. These results explain that the size selectivity observed in the experiment is due to the free energy potential well for the particles having the size that appropriately fits the void.

Importance of Ionic Entropy in Size-Selective Particle Localization. It is instructive to examine the different roles of electrostatic and entropic contributions to the trapping process. The electrostatic interaction is responsible for attracting the particles toward the void surface, but when the surfaces of the particle and nanovoid get close to each other, the EDLs of the two oppositely charged surfaces overlap and the surrounding cations and anions are depleted in the EDL-overlapping region. This phenomenon weakens the screening of surface charges and thus increases the stored electrostatic energy between those two surfaces. However, as the particle approaches the nanovoid surface, some ions from the overlapped EDL region are displaced to the free space above, thereby increasing the entropy of the system and further contributing to strong confinement force. In our cases, the entropic energy contributes much more to the final potential well and dominates the size-selective confinement, as shown in Figure 4. Also, a better geometric fit of the particle and the void will displace a larger number of ions in solution as the gap between the two surfaces closes in. This accordingly causes higher increase in entropy, which leads to deeper free energy well. A similar ion depletion process and the appearance of an electrostatic energy barrier as well as free energy wells can also be observed in a simpler system of two oppositely charged parallel surfaces (see Section S3 in the Supporting Information).

To verify this explanation, we calculate the depth of the free energy potential well experienced by the particles when they are at the lowest positions in the voids for particles of different sizes from 100 nm to 1 μm, and we also calculate the areas of overlapping EDLs between the particles and the structures. As clearly shown in Figure 5, the depth of the potential well shows direct correlation with the EDL-overlapping areas and both of these two plots expect that the nanovoid structure with current geometry works best for the 500 nm sized particles. This is because the best "particle−void" fit will create the largest overlapping area between the two surfaces, which releases the most number of ions and causes the largest entropy change. Therefore, the nanovoid shape can be optimized in order to better match particles of particular size and geometry. Furthermore, ion type and concentration can also be tuned depending on the target particles and operating environment. These perspectives were analytically investigated by the tuning of nanovoid periods (*i.e.*, 500, 700, and 900 nm) and shapes (*i.e.*, hemispherical *vs* sinusoidal nanovoids) and modulation of ionic solution as summarized in Sections S4, S5, and S6 in the Supporting Information.

CONCLUSIONS

In summary, we have developed a simple and low-cost methodology to size-selectively confine and sort the sub-micrometer particles. This is achieved by utilizing the nanovoid-directed electrostatic and entropic interactions, which realized stable trapping without any chemical linkage. A high-throughput DNI technique was used to create a 2D nanovoid patterns on the flexible substrates, where the void pattern period, depth, and shape can be tailored depending on the target particle species. We have experimentally and analytically demonstrated that the size-selective confinement of sub-micrometer particles in the nanovoids is due to the free energy change of the particle−void interaction system, which arises from the overlapping of EDLs, ionic redistribution, and the associated electrostatic and entropy energy change. Application of the size-selective particle confinement method delivered in this study could potentially be extended to scalable localization, sorting, and manipulation of charged biological objects such as proteins, lipid vesicles, cancer cells, and bacteria, as well as the sub-micrometer-sized pollutant collection. The interactions exploited in this work could even be responsible for certain nonspecific adsorption of bio-molecules on surfaces, where the interplay between nanoscale surface topography, electrostatic interaction, and entropic effects is important.

METHODS

The 700 nm period, 500 nm deep SiO_2 grating pattern having 1:1 duty (*i.e.*, ratio of line width to spacing) was fabricated on a 6 in., 500 nm thick SiO_2-coated 6 in. Si wafer, by using the nanoimprint lithography[47] followed by reactive ion etching.[48] The DNI mold was prepared by cleaving the grating-patterned SiO_2 wafer along the direction perpendicular to the grating axis, with the length of the cleaved edge of ∼2 cm. The nanovoid pattern was created on a isopropyl alcohol (IPA) cleaned PC film (DE 1-1, Clear, Makrofol) by performing the 2D-DNI process at 150 °C by using a custom-built 5-DOE DNI system.[41] The inscribing forces for the first and second DNI strokes were controlled to 1.5 and 1 N, respectively. A 10 nm thick Al_2O_3 layer was conformally coated on the 2D nanovoid-patterned surface by RF sputtering (Lab 18-2, Kurt J. Lesker), which was then assembled into the microfluidic device. The fluorescent-labeled (FITC-525 nm) PS particles (Molecular Probes, Ltd.) were centrifuged and re-aliquoted into solutions with varying ionic concentrations. The PS particle suspension at an initial volume fraction of 0.1 wt % was injected into the chamber at a fixed flow rate (10 μL/min). After 15 min allowed for equilibration, the particles in solution were imaged by using a Richter CCD combined with an Olympus BX-100 fluorescence microscope, with an exposure time of 30 ms. All SEM imaging was performed by using the Philips XL-30 FEG or JEOL JSM-6700F instruments.

ASSOCIATED CONTENT

Supporting Information

The Supporting Information is available free of charge at https://pubs.acs.org/doi/10.1021/acsnano.1c00014.

> Parametric investigation of metal oxide-coated surface charge in ionic solution, calculations of Poisson−Boltzmann equations in multivalent electrolyte solution and for two charged planar surfaces, effects of nanovoid periods and shapes, influence of the ionic concentration and ion valence, and additional comment on the deep free energy well (PDF)

AUTHOR INFORMATION

Corresponding Authors

Jong G. Ok − *Department of Mechanical and Automotive Engineering, Seoul National University of Science and Technology, Seoul 01811, Republic of Korea;* orcid.org/0000-0002-8703-2915; Email: jgok@seoultech.ac.kr

L. Jay Guo − *Applied Physics, University of Michigan, Ann Arbor, Michigan 48109, United States; Department of Electrical Engineering and Computer Science, University of Michigan, Ann Arbor, Michigan 48109, United States; Macromolecular Science and Engineering, University of Michigan, Ann Arbor, Michigan 48109, United States;* orcid.org/0000-0002-0347-6309; Email: guo@umich.edu

Authors

Long Chen − *Applied Physics, University of Michigan, Ann Arbor, Michigan 48109, United States; Department of Electrical Engineering and Computer Science, University of Michigan, Ann Arbor, Michigan 48109, United States;* Present Address: Amazon Alexa, 1120 Enterprise Way, Sunnyvale, CA 94089, USA

Ashwin Panday − *Macromolecular Science and Engineering, University of Michigan, Ann Arbor, Michigan 48109, United States;* Present Address: Micron Technology, Inc., 8000 South Federal Way, Boise, ID 83707, USA.

Jonggab Park − *Department of Mechanical and Automotive Engineering, Seoul National University of Science and Technology, Seoul 01811, Republic of Korea*

Mingyu Kim − *Department of Mechanical and Automotive Engineering, Seoul National University of Science and Technology, Seoul 01811, Republic of Korea*

Dong Kyo Oh − *Department of Mechanical and Automotive Engineering, Seoul National University of Science and Technology, Seoul 01811, Republic of Korea; Department of Mechanical Engineering, Pohang University of Science and Technology (POSTECH), Pohang 37673, Republic of Korea;* orcid.org/0000-0001-7025-6720

Complete contact information is available at: https://pubs.acs.org/10.1021/acsnano.1c00014

Author Contributions

L.C., A.P., and L.J.G. conceived and designed the research. L.C. and A.P. conducted most simulation and experimental works, respectively, under the supervision of J.G.O. and L.J.G. J.P., M.K., and D.K.O. contributed to the nanovoid pattern fabrication and characterization. L.C., A.P, J.G.O., and L.J.G. wrote the manuscript with all authors' assistance for figure preparation and consistent discussion. All authors read and approved the final manuscript. L.C. and A.P. contributed equally to this work.

Notes

The authors declare the following competing financial interest(s): L.C., A.P., J.G.O., and L.J.G. declare interest in an issued US Patent, No. 10,661,273.

ACKNOWLEDGMENTS

This research was supported in part by the U.S. National Science Foundation (Grant Nos. CMMI-1635636 and CMMI-1727918) and by the National Research Foundation of Korea (NRF) grants funded by the Korean Government (Nos.

2015R1A5A1037668 and 2020R1F1A1073760 (Ministry of Science and ICT (MSIT)).

REFERENCES

(1) Zeng, S. W.; Baillargeat, D.; Ho, H. P.; Yong, K. T. Nanomaterials Enhanced Surface Plasmon Resonance for Biological and Chemical Sensing Applications. *Chem. Soc. Rev.* **2014**, *43* (10), 3426−3452.

(2) Goncalves, M. R. Plasmonic Nanoparticles: Fabrication, Simulation and Experiments. *J. Phys. D: Appl. Phys.* **2014**, *47* (21), 213001.

(3) Fan, X. F.; Zheng, W. T.; Singh, D. J. Light Scattering and Surface Plasmons on Small Spherical Particles. *Light: Sci. Appl.* **2014**, *3* (6), e179.

(4) Verma, A.; Stellacci, F. Effect of Surface Properties on Nanoparticle-Cell Interactions. *Small* **2010**, *6* (1), 12−21.

(5) Lundqvist, M.; Stigler, J.; Elia, G.; Lynch, I.; Cedervall, T.; Dawson, K. A. Nanoparticle Size and Surface Properties Determine the Protein Corona with Possible Implications for Biological Impacts. *Proc. Natl. Acad. Sci. U. S. A.* **2008**, *105* (38), 14265−14270.

(6) Roldan Cuenya, B. Synthesis and Catalytic Properties of Metal Nanoparticles: Size, Shape, Support, Composition, and Oxidation State Effects. *Thin Solid Films* **2010**, *518* (12), 3127−3150.

(7) Terra, J. C. S.; Desgranges, A.; Monnereau, C.; Sanchez, E. H.; De Toro, J. A.; Amara, Z.; Moores, A. Photocatalysis Meets Magnetism: Designing Magnetically Recoverable Supports for Visible-Light Photocatalysis. *ACS Appl. Mater. Interfaces* **2020**, *12* (22), 24895−24904.

(8) Chang, F. F.; Bai, Z. Y.; Li, M.; Ren, M. Y.; Liu, T. C.; Yang, L.; Zhong, C. J.; Lu, J. Strain-Modulated Platinum-Palladium Nanowires for Oxygen Reduction Reaction. *Nano Lett.* **2020**, *20* (4), 2416−2422.

(9) Chen, W. H.; Zhou, Z. X.; Luo, G. F.; Neumann, E.; Marjault, H. B.; Stone, D.; Nechushtai, R.; Willner, I. Photosensitized H-2 Evolution and NADPH Formation by Photosensitizer/Carbon Nitride Hybrid Nanoparticles. *Nano Lett.* **2019**, *19* (12), 9121−9130.

(10) Son, Y.; Park, M.; Son, Y.; Lee, J.-S.; Jang, J.-H.; Kim, Y.; Cho, J. Quantum Confinement and Its Related Effects on the Critical Size of GeO_2 Nanoparticles Anodes for Lithium Batteries. *Nano Lett.* **2014**, *14* (2), 1005−1010.

(11) Barbagiovanni, E. G.; Lockwood, D. J.; Simpson, P. J.; Goncharova, L. V. Quantum confinement in Si and Ge Nanostructures: Theory and Experiment. *Appl. Phys. Rev.* **2014**, *1* (1), 011302.

(12) Bai, L.; Xie, Z. Y.; Wang, W.; Yuan, C. W.; Zhao, Y. J.; Mu, Z. D.; Zhong, Q. F.; Gu, Z. Z. Bio-Inspired Vapor-Responsive Colloidal Photonic Crystal Patterns by Inkjet Printing. *ACS Nano* **2014**, *8* (11), 11094−11100.

(13) Kim, S.-H.; Lee, S. Y.; Yang, S.-M.; Yi, G.-R. Self-Assembled Colloidal Structures for Photonics. *NPG Asia Mater.* **2011**, *3* (1), 25−33.

(14) Yan, H.; Melosh, N. Nanoparticles Make Salty Circuits. *Nat. Nanotechnol.* **2016**, *11* (7), 579−580.

(15) Farcau, C.; Moreira, H.; Viallet, B.; Grisolia, J.; Ressier, L. Tunable Conductive Nanoparticle Wire Arrays Fabricated by Convective Self-Assembly on Nonpatterned Substrates. *ACS Nano* **2010**, *4* (12), 7275−7282.

(16) Chen, X.; Yang, X.; Fu, W.; Xu, M.; Chen, H. Enhanced Performance of Polymer Solar Cells with a Monolayer of Assembled Gold Nanoparticle Films Fabricated by Langmuir−Blodgett Technique. *Mater. Sci. Eng., B* **2013**, *178* (1), 53−59.

(17) Viero, Y.; Copie, G.; Guérin, D.; Krzeminski, C.; Vuillaume, D.; Lenfant, S.; Cleri, F. High Conductance Ratio in Molecular Optical Switching of Functionalized Nanoparticle Self-Assembled Nanodevices. *J. Phys. Chem. C* **2015**, *119* (36), 21173−21183.

(18) Born, B.; Krupa, J. D. A.; Geoffroy-Gagnon, S.; Holzman, J. F. Integration of Photonic Nanojets and Semiconductor Nanoparticles for Enhanced All-Optical Switching. *Nat. Commun.* **2015**, *6* (1), 8097.

(19) Si, G.; Zhao, Y.; Lv, J.; Lu, M.; Wang, F.; Liu, H.; Xiang, N.; Huang, T. J.; Danner, A. J.; Teng, J.; Liu, Y. J. Reflective Plasmonic Color Filters Based on Lithographically Patterned Silver Nanorod Arrays. *Nanoscale* **2013**, *5* (14), 6243−6248.

(20) Saeidi, C.; van der Weide, D. Bandwidth-Tunable Optical Spatial Filters with Nanoparticle Arrays. *Opt. Express* **2014**, *22* (10), 12499−12504.

(21) Sankar, M. U.; Aigal, S.; Maliyekkal, S. M.; Chaudhary, A.; Anshup; Kumar, A. A.; Chaudhari, K.; Pradeep, T. Biopolymer-Reinforced Synthetic Granular Nanocomposites for Affordable Point-of-Use Water Purification. *Proc. Natl. Acad. Sci. U. S. A.* **2013**, *110* (21), 8459.

(22) Zhao, X.; Hilliard, L. R.; Mechery, S. J.; Wang, Y.; Bagwe, R. P.; Jin, S.; Tan, W. A Rapid Bioassay for Single Bacterial Cell Quantitation Using Bioconjugated Nanoparticles. *Proc. Natl. Acad. Sci. U. S. A.* **2004**, *101* (42), 15027.

(23) Hanske, C.; Hill, E. H.; Vila-Liarte, D.; Gonzalez-Rubio, G.; Matricardi, C.; Mihi, A.; Liz-Marzan, L. M. Solvent-Assisted Self-Assembly of Gold Nanorods into Hierarchically Organized Plasmonic Mesostructures. *ACS Appl. Mater. Interfaces* **2019**, *11* (12), 11763−11771.

(24) He, J.; Boegli, M.; Bruzas, I.; Lum, W.; Sagle, L. Patterned Plasmonic Nanoparticle Arrays for Microfluidic and Multiplexed Biological Assays. *Anal. Chem.* **2015**, *87* (22), 11407−11414.

(25) Urban, A. S.; Lutich, A. A.; Stefani, F. D.; Feldmann, J. Laser Printing Single Gold Nanoparticles. *Nano Lett.* **2010**, *10* (12), 4794−4798.

(26) Kraus, T.; Malaquin, L.; Schmid, H.; Riess, W.; Spencer, N. D.; Wolf, H. Nanoparticle Printing with Single-Particle Resolution. *Nat. Nanotechnol.* **2007**, *2* (9), 570−576.

(27) Sajeesh, P.; Sen, A. K. Particle Separation and Sorting in Microfluidic Devices: A Review. *Microfluid. Nanofluid.* **2014**, *17* (1), 1−52.

(28) Yamada, M.; Nakashima, M.; Seki, M. Pinched Flow Fractionation: Continuous Size Separation of Particles Utilizing a Laminar Flow Profile in a Pinched Microchannel. *Anal. Chem.* **2004**, *76* (18), 5465−5471.

(29) McGrath, J.; Jimenez, M.; Bridle, H. Deterministic Lateral Displacement for Particle Separation: A Review. *Lab Chip* **2014**, *14* (21), 4139−4158.

(30) Blom, M. T.; Chmela, E.; Oosterbroek, R. E.; Tijssen, R.; van den Berg, A. On-Chip Hydrodynamic Chromatography Separation and Detection of Nanoparticles and Biomolecules. *Anal. Chem.* **2003**, *75* (24), 6761−6768.

(31) Ivanov, M. R.; Bednar, H. R.; Haes, A. J. Investigations of the Mechanism of Gold Nanoparticle Stability and Surface Functionalization in Capillary Electrophoresis. *ACS Nano* **2009**, *3* (2), 386−394.

(32) Barik, A.; Chen, X. S.; Oh, S. H. Ultralow-Power Electronic Trapping of Nanoparticles with Sub-10 nm Gold Nanogap Electrodes. *Nano Lett.* **2016**, *16* (10), 6317−6324.

(33) Hughes, R. A.; Menumerov, E.; Neretina, S. When Lithography Meets Self-Assembly: A Review of Recent Advances in the Directed Assembly of Complex Metal Nanostructures on Planar and Textured Surfaces. *Nanotechnology* **2017**, *28* (28), 282002.

(34) Dou, Y. Y.; Wang, B. S.; Jin, M. L.; Yu, Y.; Zhou, G. F.; Shui, L. L. A Review on Self-Assembly in Microfluidic Devices. *J. Micromech. Microeng.* **2017**, *27* (11), 113002.

(35) Lu, Y. Q.; Lin, J. P.; Wang, L. Q.; Zhang, L. S.; Cai, C. H. Self-Assembly of Copolymer Micelles: Higher-Level Assembly for Constructing Hierarchical Structure. *Chem. Rev.* **2020**, *120* (9), 4111−4140.

(36) Liu, W. Y.; Shao, J. Y.; Jia, Y. K.; Tao, Y.; Ding, Y. C.; Jiang, H. Y.; Ren, Y. K. Trapping and Chaining Self-Assembly of Colloidal Polystyrene Particles over a Floating Electrode by Using Combined Induced-Charge Electroosmosis and Attractive Dipole-Dipole Interactions. *Soft Matter* **2015**, *11* (41), 8105−8112.

(37) Arai, N.; Watanabe, S.; Miyahara, M. T. On the Convective Self-Assembly of Colloidal Particles in Nanofluid Based on *in Situ* Measurements of Interaction Forces. *Langmuir* **2019**, *35* (35), 11533−11541.

(38) Ok, J. G.; Panday, A.; Lee, T.; Guo, L. J. Continuous Fabrication of Scalable 2-Dimensional (2D) Micro- and Nanostructures by Sequential 1D Mechanical Patterning Processes. *Nanoscale* **2014**, *6* (24), 14636−14642.
(39) Ok, J. G.; Ahn, S. H.; Kwak, M. K.; Guo, L. J. Continuous and High-Throughput Nanopatterning Methodologies Based on Mechanical Deformation. *J. Mater. Chem. C* **2013**, *1* (46), 7681−7691.
(40) Oh, D. K.; Nguyen, D. T.; Lee, S.; Ko, P.; Heo, G. S.; Yun, C. H.; Ha, T. W.; Youn, H.; Ok, J. G. Facile and Scalable Fabrication of Flexible Reattachable Ionomer Nanopatterns by Continuous Multidimensional Nanoinscribing and Low-Temperature Roll Imprinting. *ACS Appl. Mater. Interfaces* **2019**, *11* (12), 12070−12076.
(41) Oh, D. K.; Lee, S.; Lee, S. H.; Lee, W.; Yeon, G.; Lee, N.; Han, K.-S.; Jung, S.; Kim, D. H.; Lee, D.-Y.; Lee, S. H.; Park, H. J.; Ok, J. G. Tailored Nanopatterning by Controlled Continuous Nanoinscribing with Tunable Shape, Depth, and Dimension. *ACS Nano* **2019**, *13* (10), 11194−11202.
(42) Krishnan, M.; Mojarad, N.; Kukura, P.; Sandoghdar, V. Geometry-Induced Electrostatic Trapping of Nanometric Objects in a Fluid. *Nature* **2010**, *467* (7316), 692−695.
(43) Gerspach, M. A.; Mojarad, N.; Sharma, D.; Pfohl, T.; Ekinci, Y. Soft Electrostatic Trapping in Nanofluidics. *Microsyst. Nanoeng.* **2017**, *3* (1), 17051.
(44) Ruggeri, F.; Zosel, F.; Mutter, N.; Rozycka, M.; Wojtas, M.; Ozyhar, A.; Schuler, B.; Krishnan, M. Single-Molecule Electrometry. *Nat. Nanotechnol.* **2017**, *12* (5), 488−495.
(45) Ruggeri, F.; Krishnan, M. Entropic Trapping of a Singly Charged Molecule in Solution. *Nano Lett.* **2018**, *18* (6), 3773−3779.
(46) Krishnan, M. Electrostatic Free Energy for a Confined Nanoscale Object in a Fluid. *J. Chem. Phys.* **2013**, *138* (11), 114906.
(47) Chou, S. Y.; Krauss, P. R.; Zhang, W.; Guo, L. J.; Zhuang, L. Sub-10 nm Imprint Lithography and Applications. *J. Vac. Sci. Technol., B: Microelectron. Process. Phenom.* **1997**, *15* (6), 2897−2904.
(48) Kang, M.-G.; Kim, M.-S.; Kim, J.; Guo, L. J. Organic Solar Cells Using Nanoimprinted Transparent Metal Electrodes. *Adv. Mater.* **2008**, *20* (23), 4408−4413.

https://doi.org/10.1021/acsnano.1c00014
ACS Nano XXXX, XXX, XXX−XXX